Numerical and Experimental Investigation of the Interaction of Natural and Propagated Hydraulic Fracture

Fatahi, H. and Hossain, M. M. and Sarmadivaleh, M.

Journal of Natural Gas Science and Engineering 37 (2017) 409e424
http://dx.doi.org/10.1016/j.jngse.2016.11.054

Abstract

Hydraulic fracturing is extensively used to develop unconventional reservoirs, such as tight gas, shale gas and shale oil reservoirs. These reservoirs are often naturally fractured. Presence of these natural fractures can have beneficial or detrimental effects on the outcome of hydraulic fracturing operation. A proper study is required to characterize these formations, and design a suitable hydraulic fracturing operation.

This paper investigates the interaction of hydraulic and natural fractures based on numerical and experimental studies. Distinct Element Method (DEM) based numerical model has been used to simulate interaction of hydraulic and natural fractures; and the simulation results are validated through experimental studies. The experimental results are found to be in very good agreement with simulation results. The study demonstrated that the Distinct Element Method based numerical model can be used as an alternative to laboratory experiments to investigate the interaction mechanisms of hydraulic and natural fractures with greater confidence. Both experimental and numerical simulation tests showed that increasing the angle between plane of natural fracture, and direction of maximum horizontal stress increases the chance of hydraulic fracture to cross the natural fractures. At low angles, hydraulic fracture is most likely to be arrested at the plane of natural fracture; and/or cause a shear slippage at the plan of natural fracture. Natural fracture filling materials also have a great effect on the interaction mechanism. Weakly bonded natural fracture surfaces increase the chance of shear slippage to occur, and arrest the propagation of hydraulic fracture even at the high angle of interaction as high as 90°.

1. Introduction

Hydraulic fracturing of oil and gas wells gained huge popularity since it was introduced by Stanoilind in 1949 [1]. This technology is essentially important for the development of shale oil and shale gas reservoirs. Often these reservoirs are naturally fractured. This characteristic causes to branch out the propagated hydraulic fracture which can be either beneficial or be detrimental to the success of hydraulic fracturing operation depending on hydraulic fracture interacted with existing natural fracture. The branch out fractures that cause more reservoir area to be exposed to hydraulic fracture is generally beneficial. However, branch outs can cause early fracture slurry dehydration and premature proppant screen out that is detrimental to success of hydraulic fracturing operation. Proper study of interaction mechanism is thus essentially important for the efficient as well as effective design of hydraulic fracturing operation. Among the important parameters that can affect the interaction mechanism are principal stresses, fluid viscosity, flow rate, sizes of natural fractures and their orientation with respect to principal stresses, properties of fracture filling material and so on. Many researchers tried to solve this mystery either by laboratory experiments [2-12], field experiments [13-15], analytical methods [4, 5, 7-12, 16-18] or numerical simulations [6, 17, 19-26]. Analytical studies endeavour to capture the physics of the problem and try to solve it by applying mathematical models derived using physical laws. Such mathematical models are often complex, and very challenging to derive realistic analytical solutions, especially for porous heterogeneous formation in a dynamic condition. Consequently very often such solutions are oversimplified, which generally considers homogenous elastic medium in a static scenario; and assume the hydraulic fractures are already intersected the natural fracture. However, the propagation of hydraulic fracture is a dynamic process that changes the state of stress within the rock as the fracture propagates. Fracture re-initiation may occur beyond the natural fracture or from its tips before hydraulic fracture intersects natural fracture. If the numerical solutions are based on these analytical derivations, it will suffer from the same problems. Experimental studies can be considered to be a better representation of real situation amongst different solutions. Samples can be prepared in custom mode to study the effect of different parameters on the interaction mechanism. However, these experiments are not only expensive but also extremely tedious and time consuming, which hardly efficient, especially for routine industry application. This puts constraint on the number of sensitivity analysis that can be conducted and subsequent conclusions that can be drawn. This shows that none of the aforementioned methods can be used separately. Normally limited experimental studies are conducted for the calibration of numerical or analytical models. After that, numerical and analytical models are used for further sensitivity analysis to capture a wider range of situations.

Raymond et al [13, 14] and Scott et al [15] performed extensive analysis using field studies to understand fracture propagation in a coal seam gas reservoir in Queensland, Australia. They used advanced combination of petrophysical analysis to build the geomechanical model of the field and characterize presence, properties and orientation of natural fractures. They then used Gohfer software to design the hydraulic fracturing operation. Afterwards, they used a combination of radioactive tracers, sonic anisotropy logs, microseismic and tiltmeters to infer fracture initiation and propagation inside coal beds and their adjacent formations. Different monitoring systems showed consistent fracture height growth although some discrepancy between design and results as well as between results from different monitoring systems are observed.

Wu et al [24] developed a three dimensional model based on displacement discontinuity and finite element method. They considered constant fracture height; and removed the shear stress in the vertical direction. This simplified the model to be more like a 2D model (i.e. pseudo 3D). The problem of fluid flow and rock mechanical coupling was solved iteratively using Newton-Raphson and Picard iterative method. Zhang et al [23] developed a Discrete-Continuum model using PFC2d and Flac2d to investigate the interaction mechanism. They performed rigorous sensitivity analysis to study the effect of different parameters such as flow rate, fluid viscosity, material stiffness etc, on the interaction outcome. However, model results were not verified by other means such as experimental or analytical results. Keshavarzi and Jahanbakhshi [27] studied the interaction mechanism using extended finite element method (XFEM). They used the concept of energy release rate for fracture propagation and fracture behaviour at intersection point in a 2D space. Their numerical results showed good agreement with Warpinski and Teufel's experimental results [8]. Dahi Taleghani and Olson [25] also used XFEM to investigate the interaction mechanism. Similar to Keshavarzi and jahanbakhshi, they used the energy release rate for intact rock and natural fracture to determine the interaction outcome. They used this model to investigate the propagation of hydraulic fracture in presence of abundant natural fractures under different stress regimes.

Dependence of most of the numerical models on analytical results makes them prone to same errors that are present in analytical results. Meshing requirement also makes these models rigid for fracture advancement. Re-meshing requirement in some of these models such as the ones that are dependent on finite element model creates another difficulty to use these models. The distinct element method presented in this paper is found to be unique in nature as it does not depend on analytical solutions that cover the hydraulic fracturing process. Fracturing occurs as a result of decoupling between sample particles. Model results have been validated through comparison with experimental results. These experiments were conducted in True Tri-axial Stress Cell (TTSC) with the capability to impose three independent stresses on the sample.

2. Numerical Studies

Reservoir rock may contain imperfections such as faults, joints, natural fractures and so on. Simulating these rocks in Discrete Element Method (DEM) based numerical model is easier and more accurate than using a Continuum or Finite Element based numerical model. In DEM, sample is modelled as a composite of individual particles that can move and rotate with respect to each other. This eliminates the meshing requirement that is necessary in continuum based models such as Finite Element Method (FEM). In continuum based models, the way that meshes are defined can affect the accuracy of the model. In the case of fracture propagation, re-meshing is often required as the fracture tip advances. Figure 1 shows a sample that has been simulated using DEM and FEM models; and shows that in the case of DEM, no meshes were required.

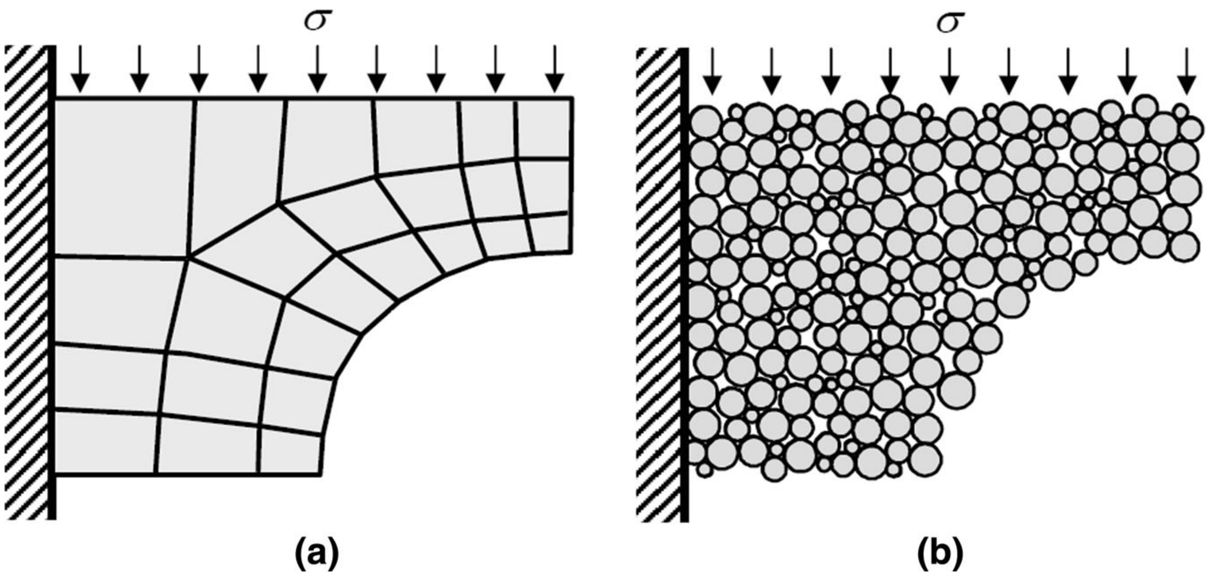

Figure 1: Sample modelled using a- Finite Element Method (FEM). b- Discrete Element Method (DEM) [28]

PFC2D is a numerical tool based on Distinct Element Method. Distinct Element method is a family of DEM. Figure 2 shows a sample that has been simulated in PFC2D. The sample is composed of grey particles. These particles are connected together using either contact or parallel bonds. The strength and stiffness of particles and bonds are adjusted to calibrate the mechanical properties of the simulated sample against real samples. Comprehensive details regarding mechanical properties calibration can be found in author's paper, Fatahi [29] and also in the Itasca manual [30]. Red lines in Figure 2 connect the centre of particles to their neighbouring particles. These red lines form polygons that are defined as domains. These domains have different volumes with respect to each other. Black circles show normalized domain volumes. The larger the circle the bigger the domain volume. Black lines connect domains to their neighbouring domains. Fluid is stored in the domains. Figure 3a shows two domains in blue and yellow colour. The red rectangle shows the imaginary parallelepiped between these two domains. Figure 3b shows the dimensions of the parallelepiped. Fluid flows between domains through this parallelepiped. Further details regarding fluid flow and calibration can be found in the paper Fatahi and Hossain [31].

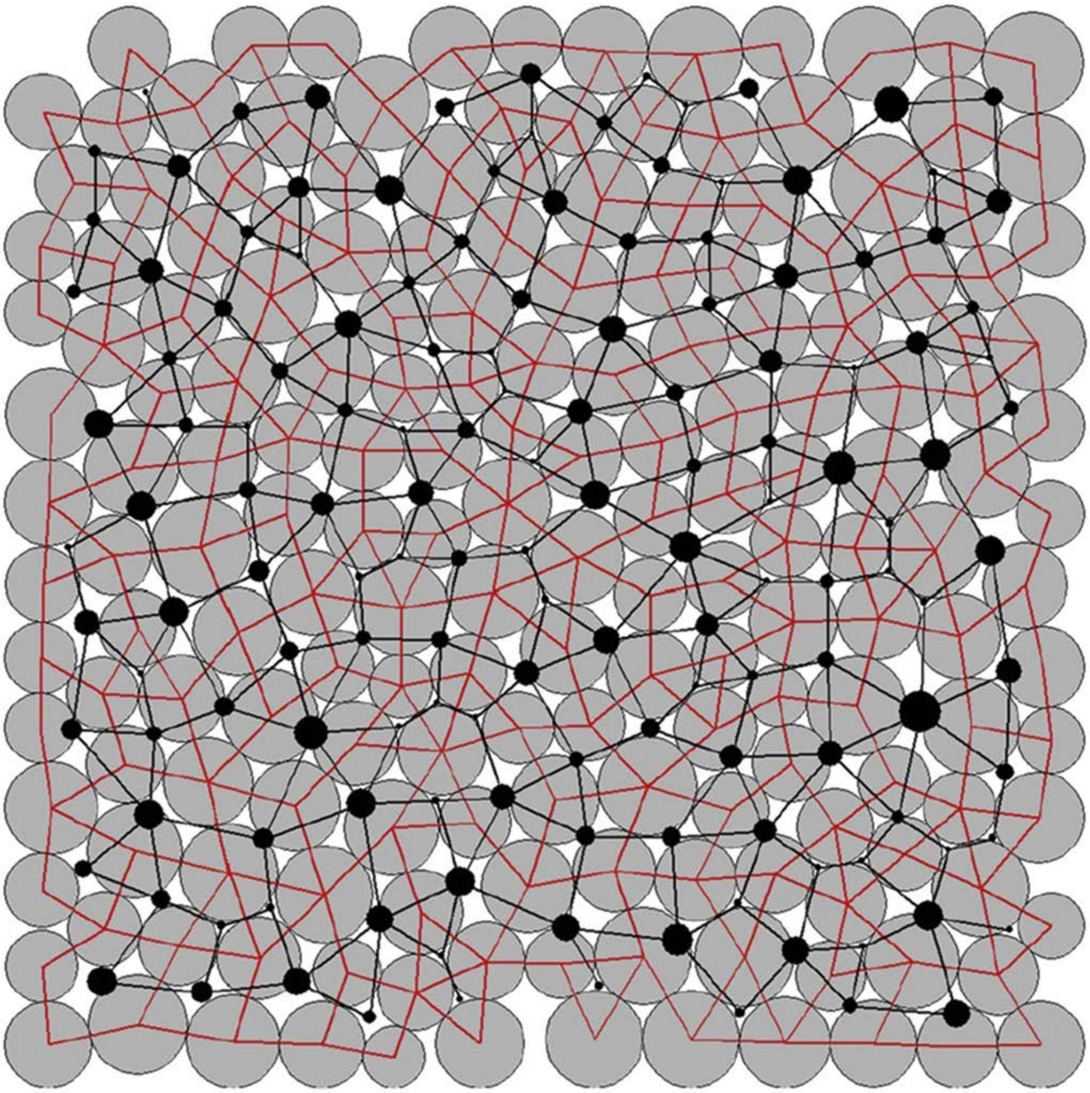

Figure 2: A sample simulated in PFC2D. Grey circles represent sample particles. Red lines connect centre of sample particles to their adjacent particles. Polygons created by these red lines are defined as domains. Black circles show the normalized size of domains with respect to largest domain size. Black lines connect domains to their neighbouring domains. [31]

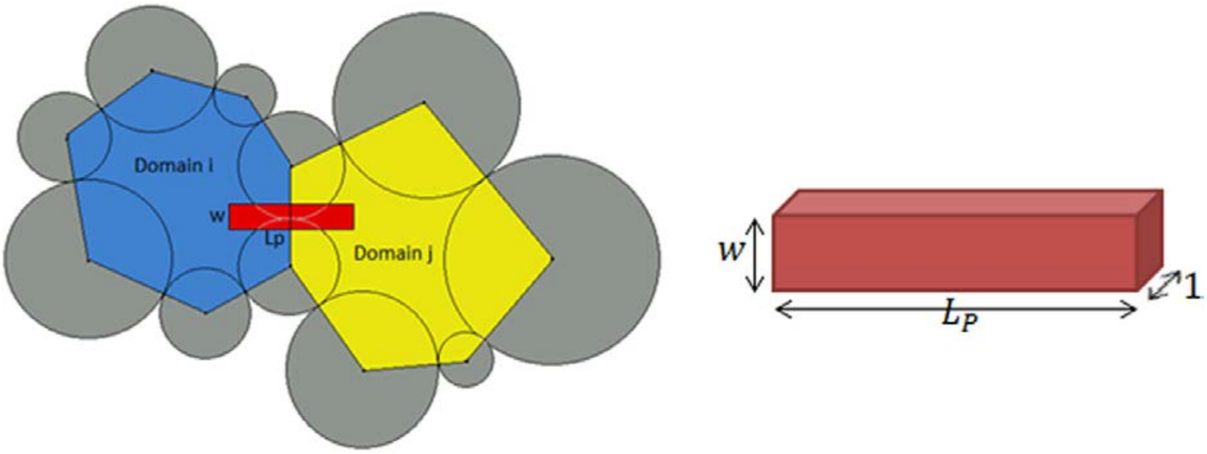

(a) (b)

Figure 3: a- Two domains shown in blue and yellow colour. Fluid flows between them through the red pipe. b- Pipe for fluid flow between domains. Its length is L_P, height is w and width is 1. [31]

Natural fractures are simulated by replacing contact or parallel bonds by smooth joint bonds. Figure 4 shows two natural fractures in black coloured dashed lines in a sample that is simulated in PFC2D. Properties of smooth joints can be adjusted to calibrate natural fracture properties against real cases. These properties can be adjusted to calibrate friction and cohesion of natural fractures. Smooth joints and their properties are well explained in Itasca manual [30]. In Figure 4 wellbore is shown at the centre of the sample. Two principal stresses are applied to the sides of the sample. Hydraulic fracture is shown in red colour. Pressure is shown as blue coloured circles with larger circles showing higher pressures. As the fluid pressure in a domain increases, it puts the domain particle bonds under tension. If the tensile or shear force between the particles reaches the tensile or shear strength of the bond that joins them, the bond will break. This bond breakage is replaced by a small red line between the particles to show the hydraulic fracture. Bond breakage one after each other shows the hydraulic fracture propagation. Fatahi et al [32] studied hydraulic fracture initiation and propagation as well as calibration of initiation and breakdown pressure against experimental results in PFC2D.

The current study investigates the interaction between hydraulic and natural fracture under different conditions of smooth natural fracture properties and interaction angles. The results of the simulation are compared against experimental studies. Results demonstrate excellent match between experimental and numerical results.

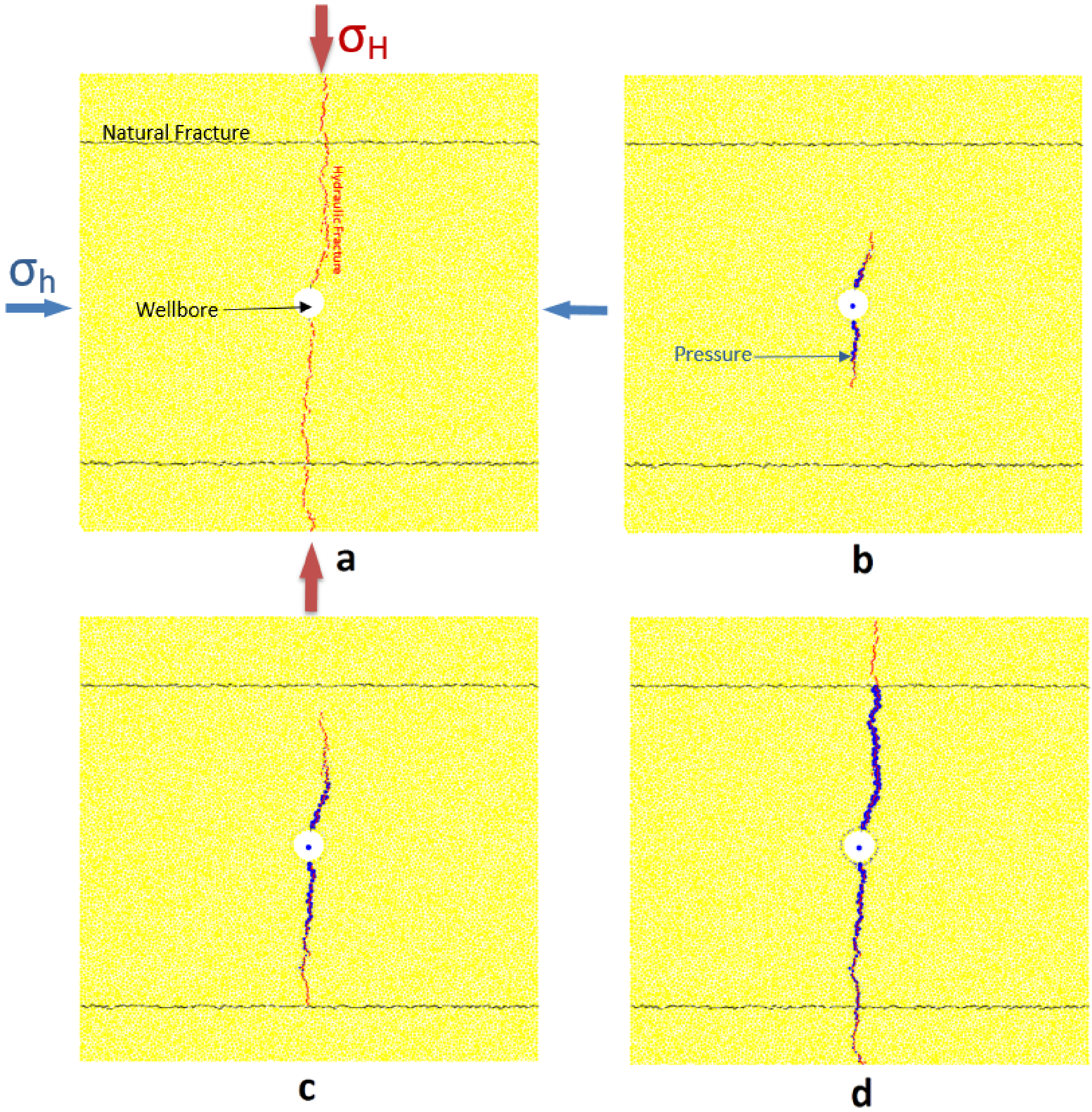

Figure 4: a) Sample in yellow colour. Natural fracture is shown as black dashed lines. Induced hydraulic fracture is shown as red dashed lines. Wellbore is shown as white circle in the middle of the sample. b) Pressure shown as blue circles. The larger the size of the circles the higher the pressure. Hydraulic fracture has not reached the natural fracture yet. c) The lower wing of hydraulic fracture arrived at natural fracture. d) Both wings of hydraulic fracture have crossed the natural fractures. Hydraulic fracture propagated in the direction of maximum horizontal stress.

Figure 5 shows colour coded pressure distribution for the sample sate of Figure 4d. Each dot shows the pressure of one domain. Circle colours show domain pressures.

It this figure, all circles have same diameter. Figure 5a shows pressure distribution versus domain X and Y position. Figure 5b shows pressure versus domain Y position. As it can be seen from Figure 4d and Figure 5, pressure in the upper wing of fracture is slightly lower than wellbore pressure. The reason is that, although hydraulic fracture crossed upper natural fracture and reached the upper boundary, but fracture beyond natural fracture didn't become wide enough to allow high fluid passage. This could be because of natural fracture slippage at upper natural fracture surface near the intersection point that prevented high stress transfer to the opposite side of natural fracture to make fracture wide enough for fluid flow. On the other hand, the lower wing of hydraulic fracture after crossing natural fracture attained some width to allow fluid passage. Also as it can be seen from the pressure profile, pressure in the lower wing is not perfectly linear and has a shape of uneven line. This is because of non-smooth profile of hydraulic fracture wall.

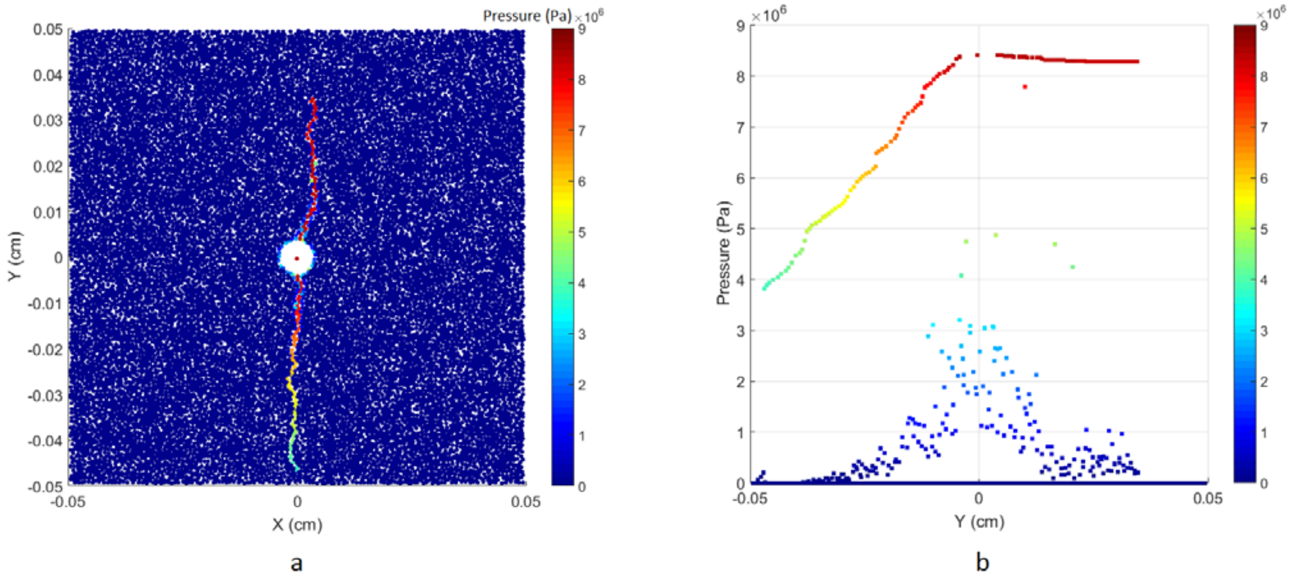

Figure 5: Colour coded pressure distribution inside sample and fracture. Each circle shows pressure of one domain. Its colour represents domain pressure. a: Pressure distribution versus domain X and Y position. b: Pressure versus domain Y position.

The current study investigates the interaction between hydraulic and natural fracture under different conditions of smooth natural fracture properties and interaction angles. The results of the simulation are compared against experimental studies. Results demonstrate excellent match between experimental and numerical results.

3. Simulation of the interaction of Hydraulic and Natural Fractures

Interaction between hydraulic and natural fractures depends on many parameters. Amongst these parameters are rock mechanical properties (e.g. Young's modulus, Poisson's ratio, Uni-axial compressive strength etc.), fracturing fluid properties (e.g. viscosity, leak off properties, bulk modulus etc.), natural fracture properties (e.g. cohesion, friction, fracture orientations, fracture sizes etc), state of stresses (e.g. insitu stresses, deviatoric stresses, stress regime etc) and the geometry of the fracture. Figure 6 shows a cartoon representation of the geometry of a simplified case that is normally studied in the laboratory. The same geometry is used in this study. In this figure wellbore is shown as white circle in the middle of the sample with diameter "R". Two natural fractures are present above and below the wellbore at a distance of "b" with lengths of "l". Hydraulic fracture is considered to be bi-wing fracture; and is shown as two red triangles filled with orange colour. The angle between hydraulic and natural fractures is considered to be ($\pi/2 - \alpha$)", where α is the angle of natural fracture with the direction of minimum horizontal stress. Sample lengths are shown as "a". Maximum and minimum horizontal stresses are shown respectively as "σ_H" and "σ_h".

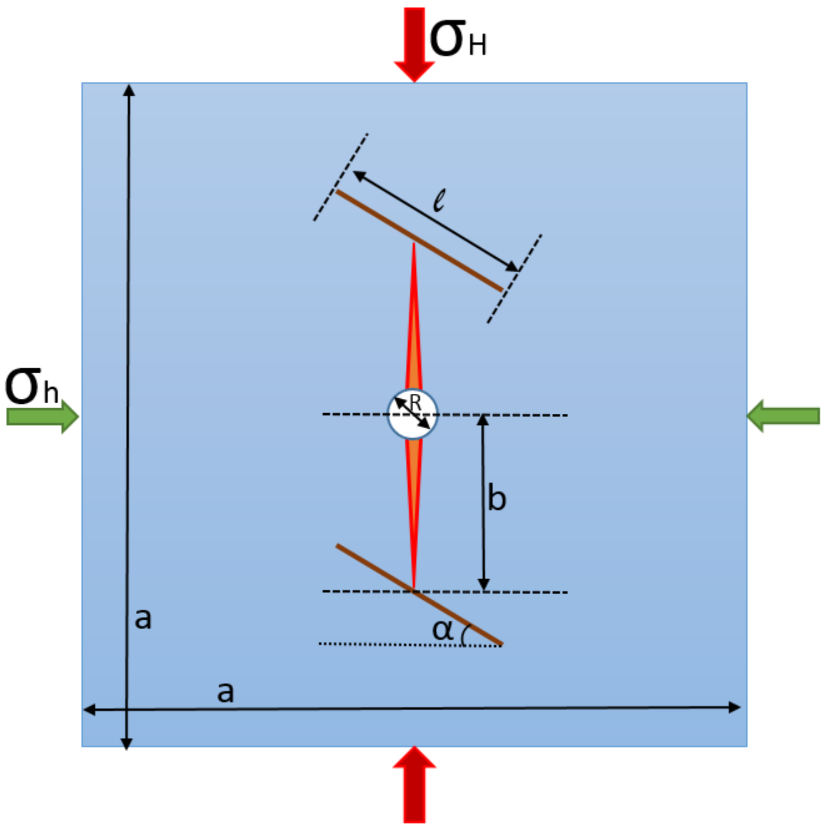

Figure 6: Geometry of a hydraulic and natural fracture interaction. a: sample dimension, b: Natural fracture distance from centre of the wellbore, R: wellbore diameter, l: natural

fracture size, α: natural fracture angle, σ_H: Maximum horizontal stress and σ_h: Minimum horizontal stress

Figure 4 shows a simulation result of the interaction between hydraulic and natural fractures at 90° angles. Figure 4a shows the final result of simulation without showing pressure. Wellbore is shown as white colour in the middle of the sample. Hydraulic fracture is shown as red dashed lines. Natural fracture is shown as black dashed lines. This figure demonstrates that hydraulic fracture propagated in the direction of maximum horizontal stress; and crossed the natural fractures. Figure 4b shows the hydraulic fracture before it arrived at natural fractures. Figure 4c shows that lower wing of hydraulic fracture arrived at natural fracture. Figure 4d shows the final simulation result with pressure shown as blue circles with different sizes. The pressure circle sizes are normalized with respect to highest pressure. The higher the pressure the bigger the circles are.

4. Experimental Studies

A rigorous experimental study was conducted to study the interaction mechanism between hydraulic fracture and natural fractures. Synthetic mortar samples were selected for this study to make sure that the only heterogeneities in the samples are the synthetic natural fractures. Real samples may have some imperfections such as hidden natural fractures or different grain diameters that can cause stress concentration. Stress concentration in one part of the sample can affect hydraulic fracture propagation and orientation, which consequently can affect test results. A ratio of one to one was considered for sand and cement weight; and a weight percentage of 40% for water to cement ratio. Mixture of water, cement and sand was mixed for 15 minutes and was poured in a Mould that was sitting on a vibratory table. Vibration intensity was controlled to make sure that there was no segregation of sand from slurry. Thin oil coated galvanized steel plates were placed in the slurry that was poured in the mould in the desired location at the desired angle to create the natural fractures. Slurry was allowed to cure for 12 hours and then was removed from the mould and placed in a water bath for 28 days. Water bath temperature was set at 25° C. Afterwards the samples were removed from the water bath; and were allowed to dry. The plates were then removed from the sample; and the sections that were separated by the plates were glued together using one of the two glues (white and brown) or cement slurry. These filling materials resemble the filling materials in the natural fractures. Figure 7 shows two samples. The left sample has natural fractures of 90° and the middle and right samples have natural fractures of 60° with respect to anticipated hydraulic fracture propagation direction. A borehole is then drilled in the middle of the sample. One side of the hole was plugged by a solid steel rod. The middle part of the hole was left open; and the other side was cased by gluing a steel pipe. Once the samples were ready, they were placed in True Triaxial Stress Cell (TTSC) (one at a time) that has the capability to impose three independent stresses on the sample to resemble vertical, minimum horizontal and maximum horizontal stresses. Fluid was then injected into the sample through still pipe at a controlled rate to pressurize the borehole. This caused a fracture initiation and propagation and eventually interaction with the pre-existing synthetic natural fractures. To get the mechanical properties of the sample, samples with similar composition and similar preparation procedures were created. After that cylindrical plugs were removed from them. Uniaxial and tri-axial tests were conducted to drive the mechanical properties of the samples. Porosity and permeability of the samples were measured on cylindrical plugs in the Poro/Permeameter apparatus. Boyle's low was used for porosity measurement and Pulse decay method was used for permeability measurements. Helium was used as the flowing fluid in these measurements. These properties as well as shear properties of glues are shown in Table 1. Shear strength of glues were determined by sandblasted aluminium lap shear test by the manufacturer; and shear property of cement was determined by direct shear test in the laboratory. Table 2 shows the mechanical properties of the synthetic and simulated samples. Further details regarding experimental study are elaborated in authors earlier studies [32-34].

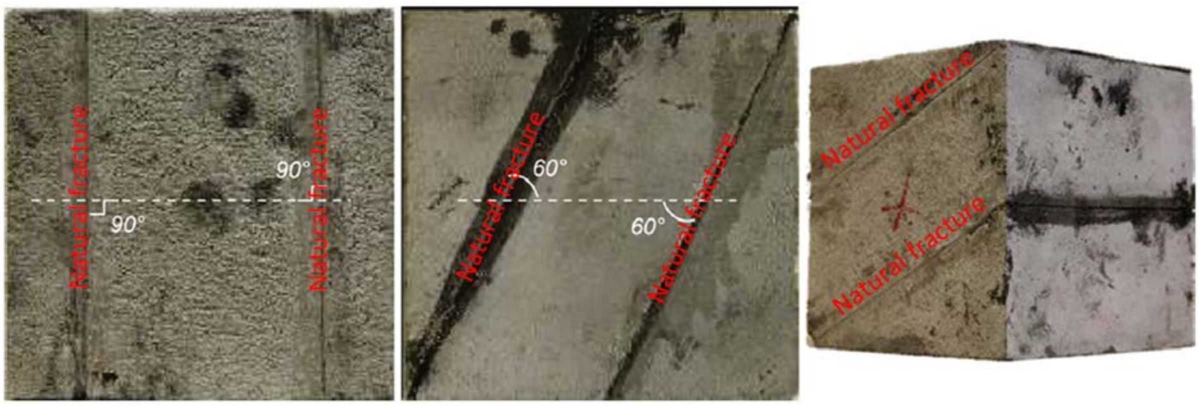

Figure 7: Two 10 cm samples with 90^{0} (left) and 60^{0} (middle and right) natural fractures with respect to anticipated hydraulic fracture direction. [34]

Table 1: Hydro-mechanical properties of synthetic sample and natural fracture filling materials. [33]

Hydro-mechanical property	Value		Test method
Uni-axial compressive Strength, UCS psi (MPa)		11,530 ±750 (79.5)	Unconfined compression test
Uni-axial poison's ratio, ν		0.197± 0.02	Unconfined compression test
Young's modulus, E, psi (GPa)		4.018×10^{6} ± 2×10^{5} (27.74)	Unconfined compression test
Internal friction coefficient, Φ (degree)		44.3	Mohr circle, confined test
Cohesion, C_c psi (MPa)		2524 (17.3)	Mohr circle, confined test
Tensile strength, T_0, psi (MPa)		510±200 (3.5)	Brazilian tensile test
Fracture toughness, K_{IC}, psi $\sqrt{in}$ (MPa$\sqrt{m}$)		710±200 (0.78)	CSB
Natural interface shear Strength, τ_0, psi (MPa)	cement	290 (2)	*sandblasted aluminum lap shear test, Provided by manufacturer
	Brown glue	*70(0.5)	
	Black glue	*145(1)	
	White glue	*3370 (26)	
Natural interface friction, μ_f		0.698±0.006	Direct Shear Test
Porosity, ϕ %		14.7±1	Two Boyle's cells
Permeability, K mD		0.018±0.005	Transient gas flood

Table 2: Synthetic and simulated sample mechanical properties

Sample Type, ID	UCS (MPa)	Young's Modulus E (GPa)	Poisson's Ratio	Cohesion (MPa)	Internal Friction coefficient (°)
Mortar	79.50	27.70	0.2	17.4	44.3
Simulated Mortar	79	27.6	0.2	17	46

To perform aluminium lap shear strength test, two aluminium plates of 2 in. width are overlapped 0.5 in. on each end of plates; and are epoxied together (Figure 8a). These two plates are then pulled apart in a direct tension test to evaluate the maximum shear strength that epoxy can tolerate. By knowing the area of epoxied surface, shear strength of epoxy is calculated by dividing shear force by shear surface area. Figure 8a shows the schematic view of the two aluminium plates that are epoxied together for lap shear test. Figure 8b shows a simulated sample, prepared to perform aluminium lap shear test. The contact strength between the particles in each of the top and bottom plates is set very high so that the plates do not fail under tensile force. The contact type between particles of top and bottom plates is set as smooth joint model. Smooth joint contact properties are then adjusted to match its shear strength against shear strength of cement and glues. For detailed information about smooth joint model and its micro-mechanical properties, please refer to PFC2D manual [30].

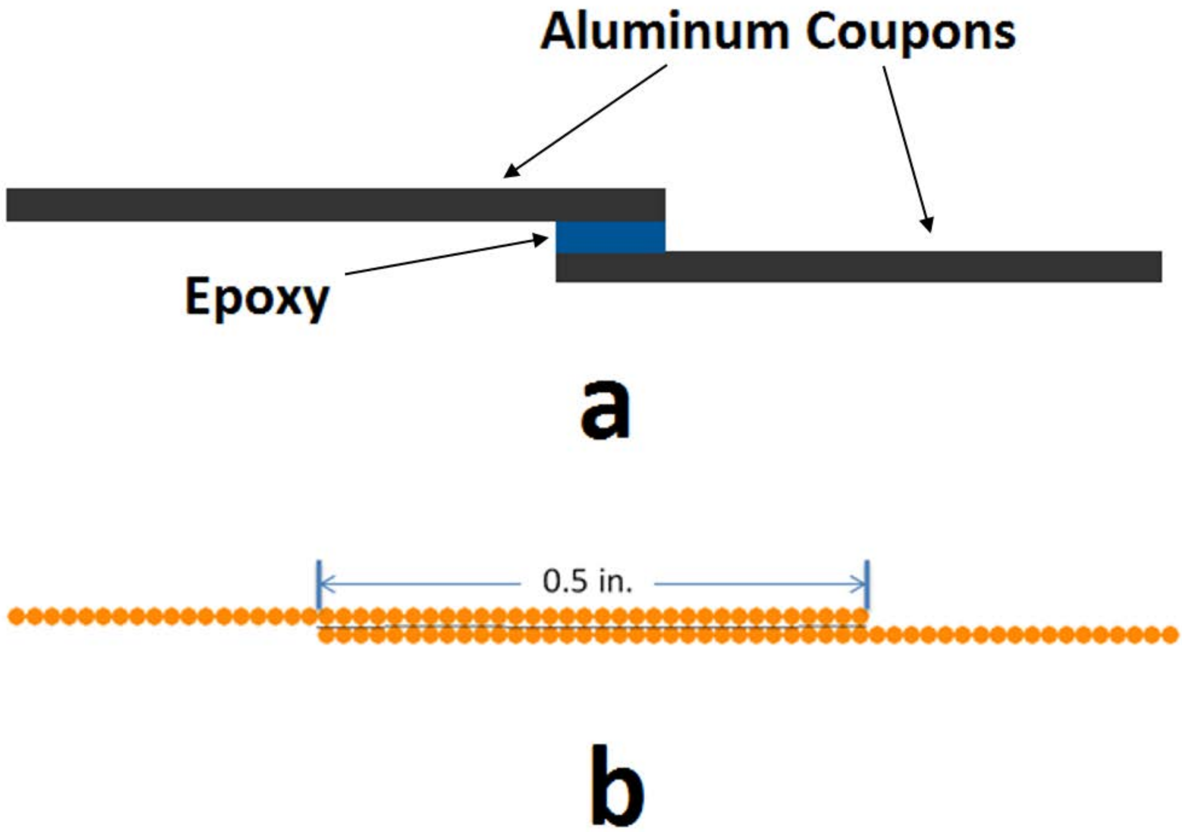

Figure 8: a) schematic view of the aluminium plates epoxied together [35] b) Simulated sample for aluminium lap shear strength test.

Table 3 shows the mechanical properties of the sooth joint contacts that simulate the filling type of material. These properties are the micro mechanical properties of the smooth joints. These micro mechanical properties were derived by trial and error to get the macro mechanical properties of the filling material that are presented in Table 1.

Table 3: Mechanical properties of smooth joint contacts simulating filling material

Parameter / Filling Material	Normal Stiffness	Shear Stiffness	Friction Coefficient	Dilation Angle	Normal strength	cohesion	Friction Angle
Unit	GPa	GPa	---	°	MPa	MPa	°
Brown Glue	1.10E+3	1.10E+3	0.1	0	1000	0.28	0.1
White Glue	1.65E+3	1.65E+3	0.7	0	1000	16	0.1
Cement	1.80E+4	1.80E+4	0.7	0	1000	60	66

5. Scaling analysis

One of the important parameters that need to be considered while doing laboratory experiments is the scaling of these tests. Tests in laboratory are performed on samples that are in centimetre scale. Field cases are in the scale of few hundred meters. As a result a dimensional analysis needs to be performed to scale down field cases to laboratory conditions. Laboratory experiments in this study are based on Sarmadivaleh's [33] scaling analysis and is explained briefly here. Early laboratory experiments didn't take into account this issue and performed experiments with field parameters. For example they used oil or water as fracturing fluid [2, 3, 6, 8, 36-45]. Even though oil was used in viscosity range of up to 3000 cp [43], but this viscosity is very low for laboratory applications. A viscosity of 3000 cp is very high for field cases and normally is associated with very viscous cross linked gel fluids. As Zoback [46] mentioned in his book and shown in Figure 9, once the fractures moves away from wellbore, the toughness or strength of the rock has minimal effect on hydraulic fracture propagation. In this figure it can be seen that once the fracture length is 1 meter, the difference in net pressures between a very strong sandstone and a weak sandstone is only 25 psi.

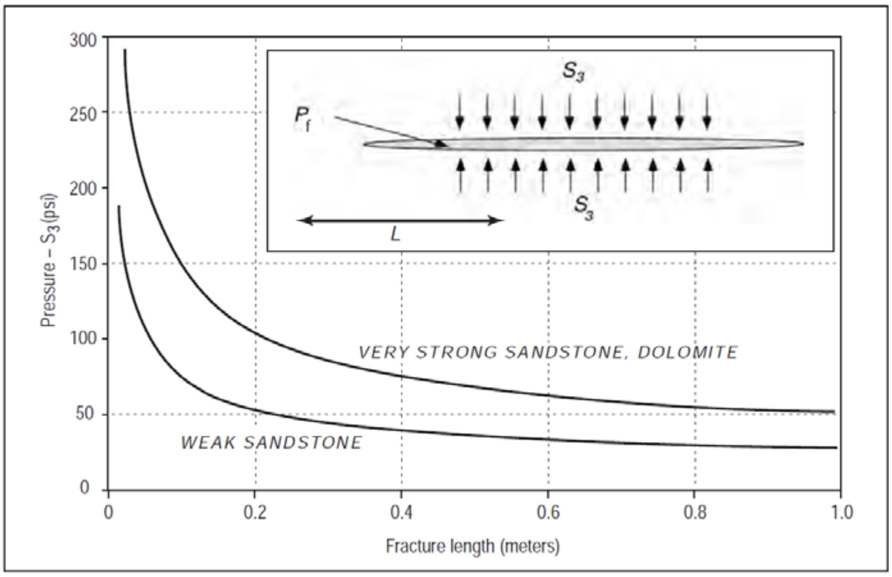

Figure 9: Fracture net pressure versus fracture length. [46]

In the field applications in the early stages hydraulic fracturing is toughness dominated. But as the fracture grows, it changes to viscous dominated. To be able to capture this phenomenon, a high viscosity fracturing fluid with low injection rate needs to be used. Figure 10 shows the scaling analysis that this study is based on.

Horizontal axis shows injection rate and vertical axis shows mode I rock fracture toughness based on Equation 1 [47]:

$$K_{IC} < 2P_n\sqrt{\frac{r_f}{\pi}} \qquad \text{Equation 1}$$

The parameters corresponding to black circle are used for the tests. This corresponds to an injection rate of 0.1 cc/min and a viscosity value of 97700 cp. This clearly indicates that this viscosity is one to two orders of magnitude larger than viscosity ranges that were used in early experimental tests. The high viscosity value and low injection rate also ensure that fracturing mechanism is controlled and stays within sample boundaries. Once the scaling laws capture the physical phenomenon that occurs in the field; field and laboratory experiments should generate the same results and laboratory results can replicate what will happen in the field.

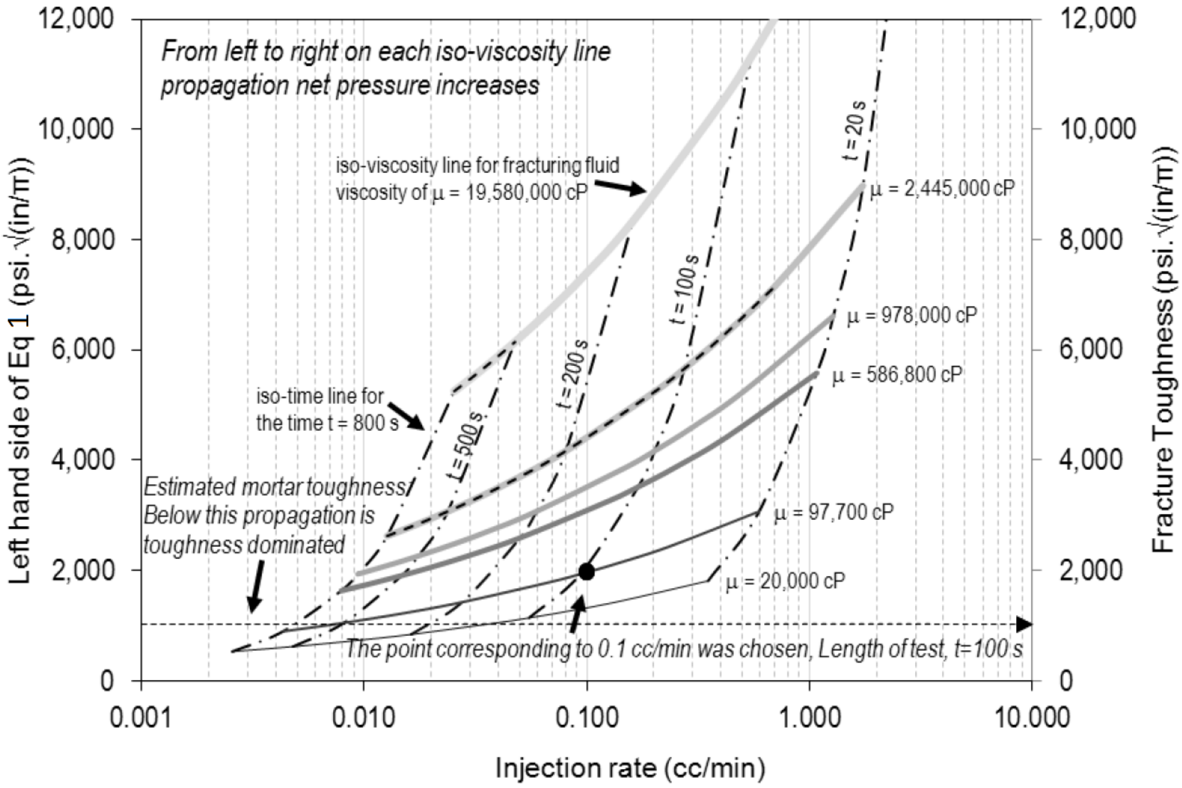

Figure 10: Scaling analysis for a 10 cm sample. For this study the parameters corresponding to the black circle are used. Modified after [33]

6. Results and discussion

This section presents the results of the interaction mechanism between the induced hydraulic fracture and natural fractures. Simulated results are compared with experimental results for different interface filling material and different interaction angles between natural and propagated hydraulic fractures. Note the term "angle" especially in this section will refer to angle between the propagated hydraulic fracture and natural fracture.

Figure 11 shows the results for the interaction angle of 90^o. In this test, the filling material is Brown Glue. Figure 11a and Figure 11c show the experimental results and Figure 11b shows the simulated result. Both simulation and experimental results demonstrated that propagated hydraulic fractures are arrested at intersection points with natural fractures. Figure 11c shows the sample with slabs detached from the main section using chisel and hammer. Main section is also split in half on the hydraulic fracture plane to describe the fracturing surface. Minor opening at intersection point is observed in slab A, whereas slab "B" shows complete arrest of hydraulic fracture. This slab was broken during detachment process. Main section "C" shows a bi-wing hydraulic fracture.

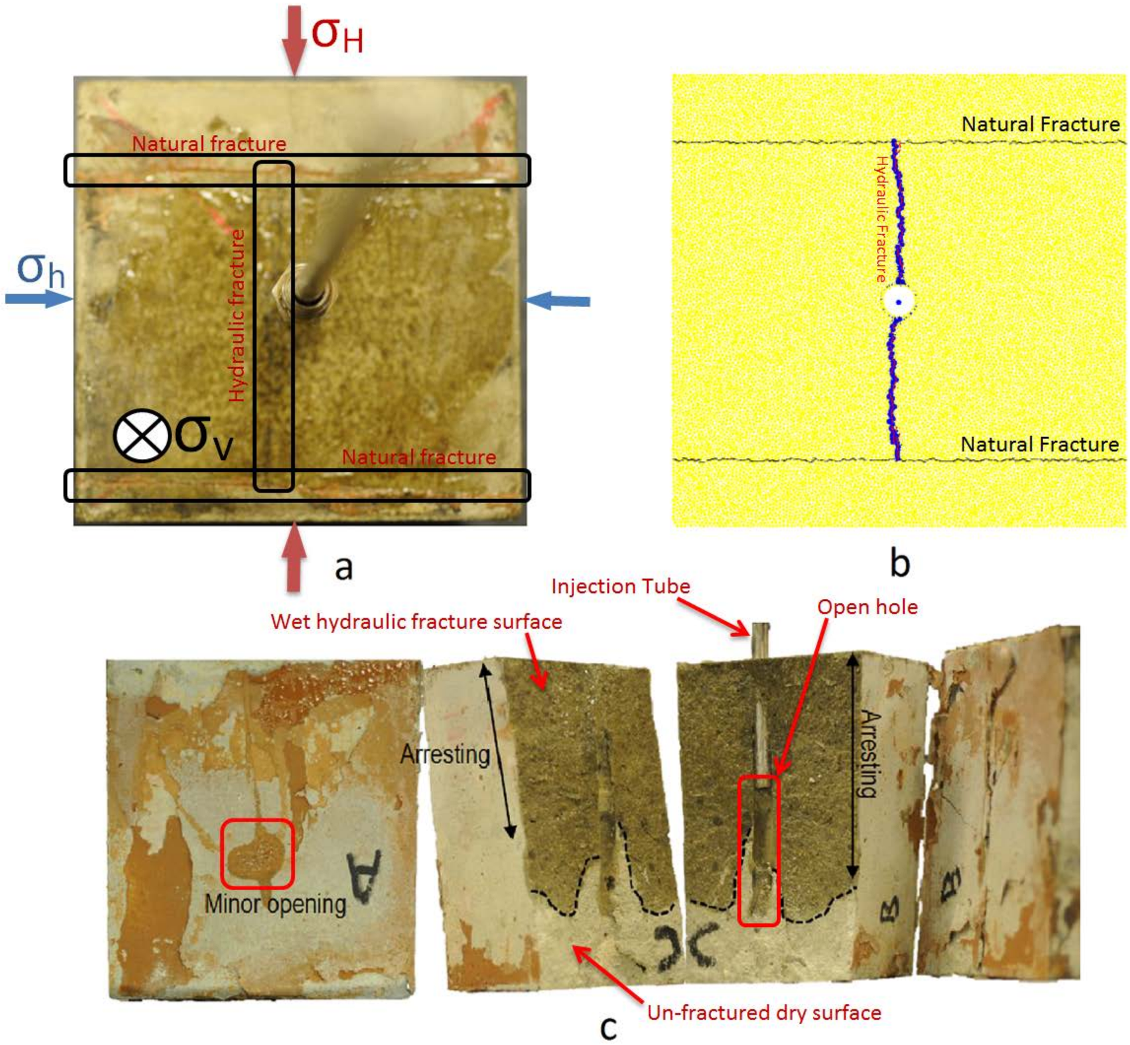

Figure 11: Brown glue as natural fracture filling material. a) Top view of the sample. Hydraulic fracture arrived at natural fracture at 90^{o}. Hydraulic fracture arrested at natural fractures. b) Simulated sample. It shows that hydraulic fracture is arrested at natural fractures. c) Sample opened to show the created hydraulic fracture. Slab "A" shows mainly arresting of the hydraulic fracture with minor opening. Slab "B" shows complete arresting of hydraulic fracture. The slab was broken while trying to detach it from main section 'C". Section "C" shows a bi-wing hydraulic fracture with fracture surface shown in dark grey colour as the fracturing fluid caused wetting of the fracture surface. Modified after [33]

Figure 12 shows a sample with white glue as natural fracture filling material. Two tests were carried out with this sample. In the first test as shown in Figure 12a, principal stresses were imposed in a way that hydraulic fracture initiated and propagated in a direction of 30^{o} with respect to natural fracture. No interaction was observed between hydraulic fracture and natural fractures. Figure 12b shows a simulation of this test with same result of no interaction. To facilitate the creation of hydraulic fractures, two sets of small notches on borehole wall were created for both experimental and simulation tests. These two sets were orthogonal. Hydraulic fracture initiated and propagated in the direction of maximum horizontal principal stress as one would anticipate. Figure 12c shows the result of second test. In this test, the principal horizontal stresses were rotated 90^o with respect to test in Figure 12a (i.e. hydraulic fracture propagated in the direction of maximum horizontal stress), and minimum horizontal stress was halved. It is observed that the hydraulic fracture propagated in the direction of maximum horizontal stress and intersected the natural fracture at about 60^o. Both wings of hydraulic fracture crossed natural fractures. The right wing shows a small offsetting at intersection point. Figure 12d shows the simulated test condition with same interaction results. Figure 12d shows that blue circles which represent pressure are higher in the first created fracture (vertical fracture) away from wellbore. This implies that pressure inside vertical fracture is higher than both wellbore pressure and pressure inside horizontal fracture. The reason is that after vertical fracture wings hit the top and bottom boundaries, the direction of principal stresses were changed. The new higher stress acted on vertical fracture walls and caused the fracture to close down. Fluid that was trapped inside fracture, experienced higher stresses from fracture walls and its pressure started to increase because of reduction in fracture volume and low compressibility of fracturing fluid. As it can be seen that the fracture wings were pinched out from both boundaries and wellbore sides. It should be noted that the size of circles that show fluid pressure are normalized based on highest pressure during each time step. Initially during fracture initiation and propagation, wellbore pressure might be the highest pressure. But if multiple fractures are present in the system, one of them may pinches out/closes and traps fluid, while other fracture/fractures propagate and cause the reduction of wellbore pressure. In this instance wellbore pressure may reduce below fluid pressure that is trapped in the pinched out fracture.

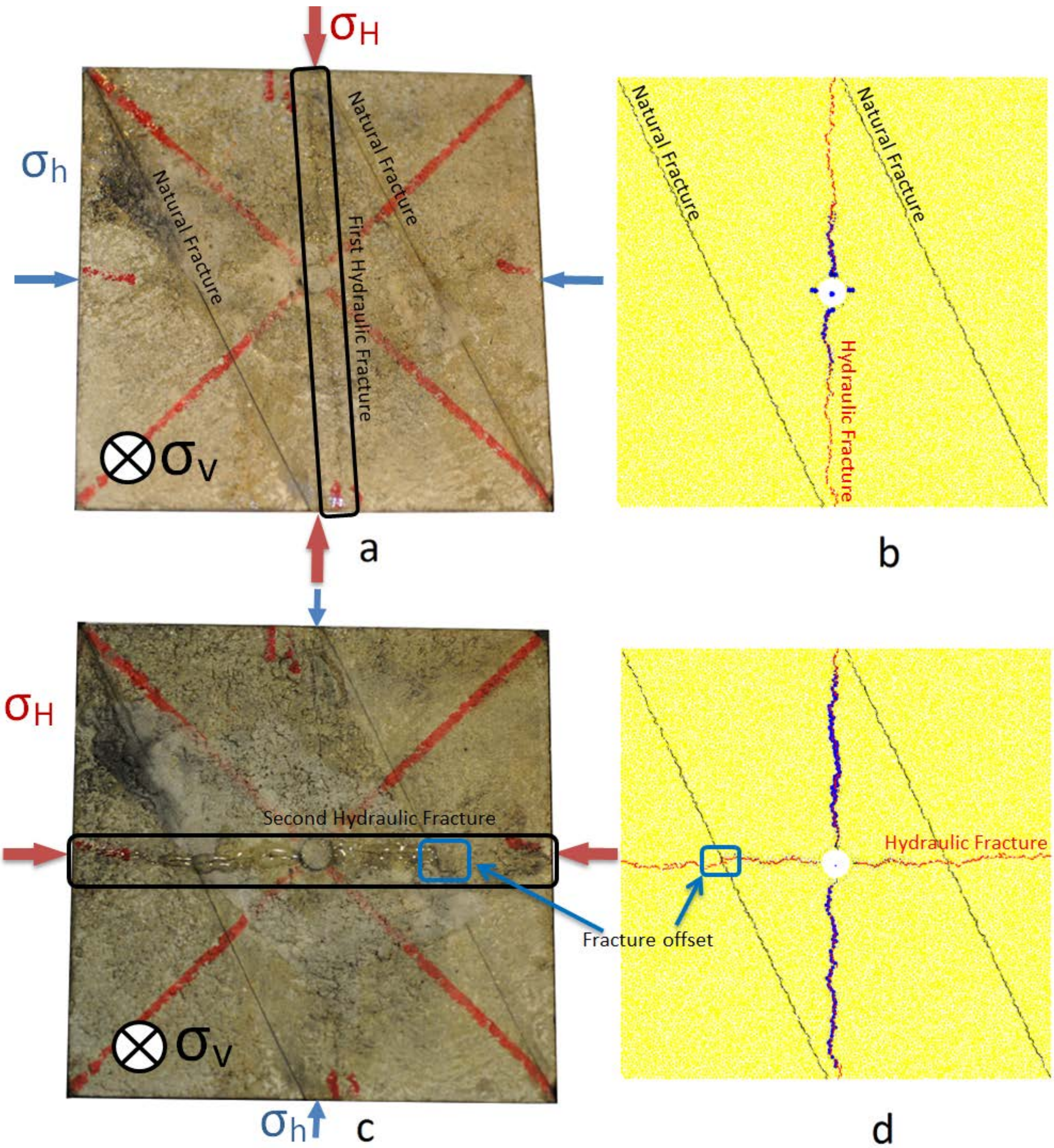

Figure 12: White Glue as natural fracture filling material. a) Experimental result for natural fracture at 30^o with respect to hydraulic fracture. No interaction between hydraulic fracture and natural fracture occurred. b) Simulated fracturing test for the natural fracture at 30^o with respect to hydraulic fracture. No interaction between hydraulic fracture and natural fracture occurred. c) Experimental result for natural interface at 60^o with respect to hydraulic fracture. Hydraulic fracture crossed natural fracture with small offset at right wing. d) Simulated fracturing test for the natural fracture at 60^o with respect to hydraulic fracture. Hydraulic fracture crossed natural fracture with small offset at left wing.

Figure 13 shows the simulation and experimental results for two cases of 0^o and 90^o orientation of natural fractures with respect to hydraulic fracture. Cement is natural fracture filling material for both samples. Figure 13a shows the experimental result for the case that hydraulic fracture was initiated and propagated parallel to natural fracture. Figure 13b shows the simulation with same interaction result. Both simulation and experimental results show that created hydraulic fracture is bi-wing in the direction of maximum horizontal stress. Figure 13c shows the experimental result for the case of 90^o interaction angle. The top wing is arrested at intersection point and bottom wing crossed the natural fracture. Figure 13d shows the simulation result for 90^o interaction angle. Simulation shows that hydraulic fracture has crossed both top and bottom natural fractures. The discrepancy between experimental and simulation results at top natural fracture is due to the fact that in the experimental case, after hydraulic fracture crossed the bottom boundary, it also intersected the boundary perpendicular to vertical stress direction. Fluid has leaked off at three boundaries and caused rapid depressurization of fracture fluid as well as loss of pressure energy. Consequently available remaining energy of fracturing fluid was not good enough to cross the top boundary. In the simulated sample, no leak off is considered in the out of plane dimension, which is considered to be a better representation of field condition. In this case that target formation is considered to be bounded within two impermeable formations on top and bottom. It is very unlikely to fracture if the top and bottom formations have higher stresses contrast with respect to target formation. The chance of splitting at interface between formations in the horizontal plane is also very slim as overburden stress will clamp it down. The net result is that fracture would be bounded in the target formation and fracturing fluid would not lose its energy readily as it did in the experimental test.

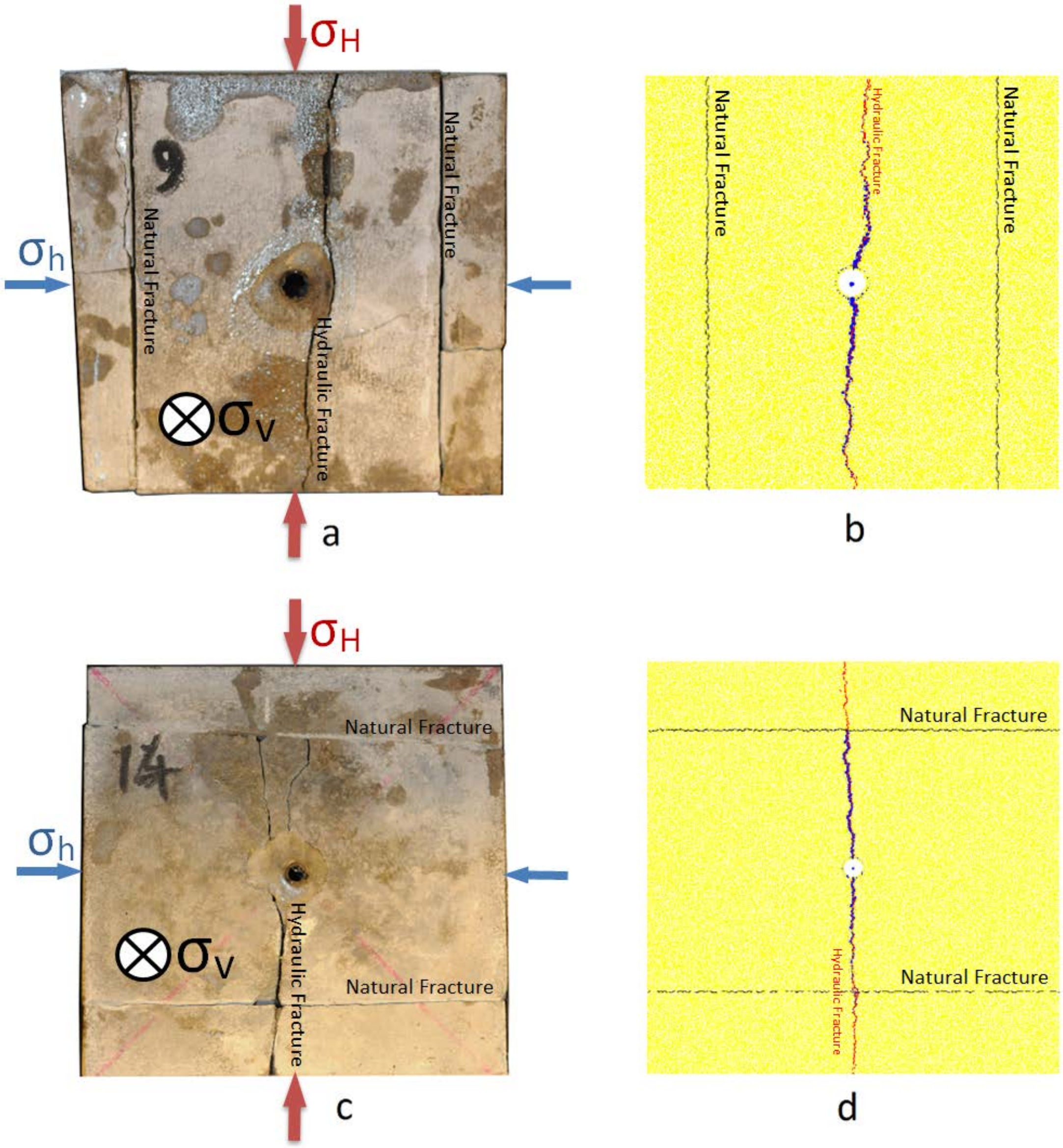

Figure 13: Cement as natural fracture filling material. a) Experimental result for natural fracture at 0^o with respect to hydraulic fracture. No interaction between hydraulic fracture and natural fractures occurred. b) Simulated fracturing test for the natural fracture at 0^o with respect to hydraulic fracture. No interaction between hydraulic fracture and natural fractures occurred. c) Experimental result for natural fracture at 90^o with respect to hydraulic fracture. Top wing arrested at intersection point. Bottom wing crossed natural fracture. d) Simulated result for natural fracture at 90^o with respect to hydraulic fracture. Both wings crossed natural fractures.

Figure 14 shows two tests for anticipated interaction angles of 60^{o} and 30^{o}. Figure 14a shows the experimental result for the anticipated 60^{o} interaction angle. As predicted fracture has arrived at natural fracture at 60^{o}. The left wing got arrested and the right wing crossed the natural fracture. Same as previous case, excessive leak off at three boundaries caused early depressurization of fracturing fluid. This caused left wing to be arrested. Figure 14b shows the simulation result for 60^{o} interaction angle. It shows that both wings crossed the natural fractures with some degree of offsetting. Offset is larger at left wing. Figure 14c shows the experimental result for the planned interaction angle of 30^{o}. However, hydraulic fracture did not propagate in the planned direction. Few parameters could cause this deviation of hydraulic fracture from the planned direction such as improper stress installation, defects in the sample and misalignment of side slabs. The main reason could be that opposite sample sides were not totally parallel. When the side slabs were cemented to the centre piece, small misalignment could cause stress to be imposed more on the side slabs. This could cause stress rotation in the centre piece, which can impact fracture initiation point and its propagation path. It then arrested at natural fractures and caused shear slippage on natural fractures. Figure 14d shows the simulation result. From this figure it can be seen that fracture initiated and propagated in the planned direction parallel to maximum horizontal stress and 30^{o} with respect to natural fractures. Hydraulic fracture arrested at natural fractures. It caused some shear slippage on natural fractures surfaces. To be able to benefit from the experimental result even though the whole physics of the problem could not be captured, a simulation was prepared with three natural fractures as shown in Figure 14e. Two natural fractures where positioned at 30° with respect to maximum horizontal stress and the third one was positioned in the direction of experimental hydraulic fracture. In this way, third natural fracture allowed the fracturing fluid to arrive at the interaction points similar to experimental result. The aim was to observe whether the fluid pressurization will cause initiation of fracture at intersection point on the opposite side of natural fracture or it causes shear slippage at natural fractures. Fluid caused shear slippage on 30° natural fractures similar to what was observed in the experimental case.

This test further confirmed the consistency between simulation and experimental results.

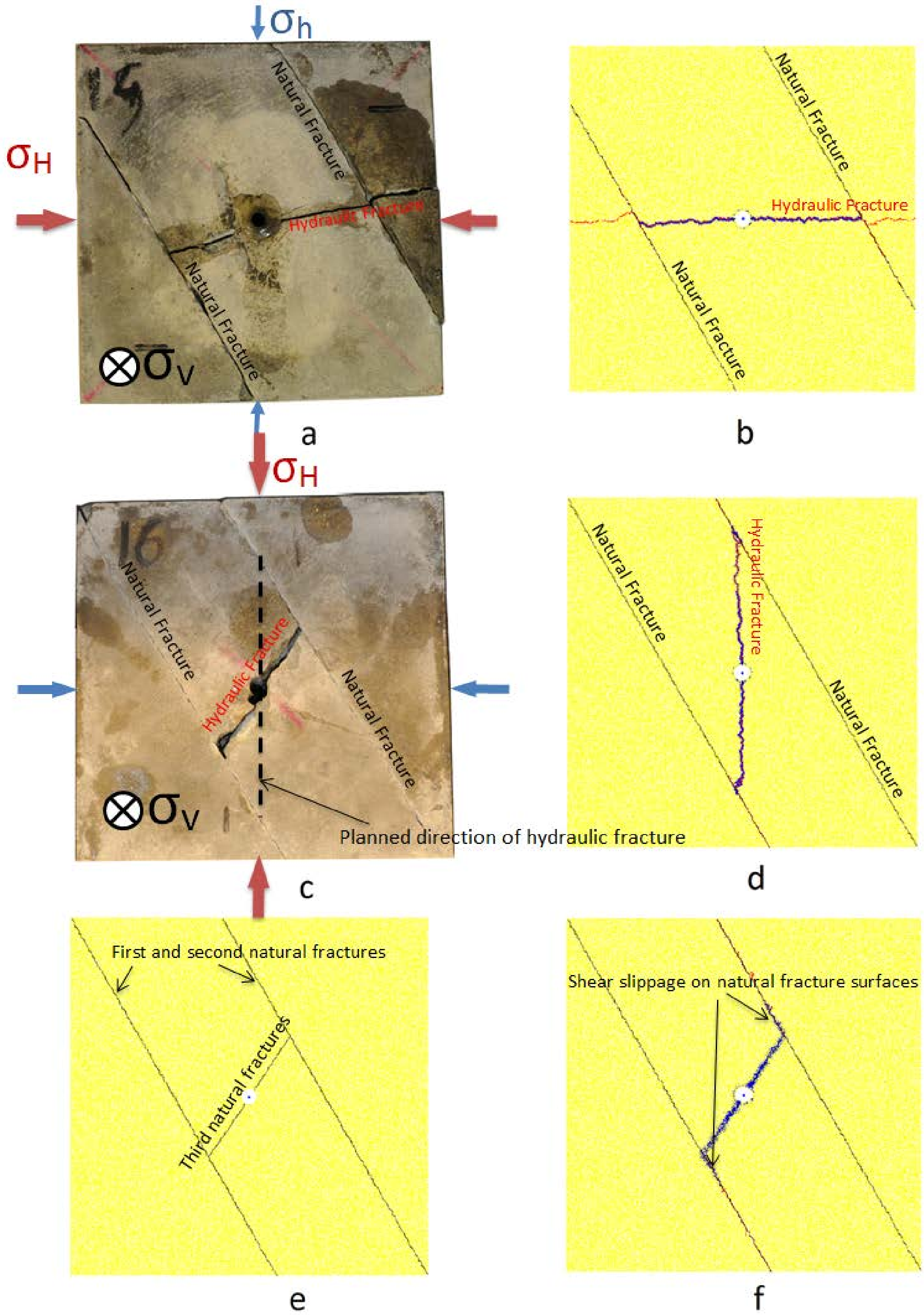

Figure 14: Cement as natural fracture filling material. a) Experimental result for natural fracture at 60^{o} with respect to hydraulic fracture. Left wing of hydraulic fracture arrested at intersection point and right wing crossed natural fracture. b) Simulated fracturing test for the natural fracture at 60^{o} with respect to hydraulic fracture. Both wings crossed natural fractures with small offsetting. Offset is larger at left wing. c) Experimental result for natural fractures at anticipated 30^{o} with respect to hydraulic fracture. Hydraulic fracture didn't propagate in the desired direction. Both wings were arrested by natural fractures. d) Simulated result for anticipated natural fracture at 30^{o} with respect to hydraulic fracture. Both wings arrested at natural fractures. Shear slippage occurred at some interval over natural fracture surfaces. e) Two natural fractures at 30° and third one in the direction of experimental hydraulic fracture. f) Shear slippage at natural fracture surfaces.

Figure 15a shows contact forces between particles at top left hand corner of sample with a natural fracture at 90° with respect to the direction of "σ_H". Blue lines show compressive forces between particles with thicker lines showing higher stresses. This figure shows that thicker lines are aligned in the direction of "σ_H" as is expected. Figure 15b shows compressive forces between particles around wellbore when the hydraulic fracture moved a small distance away from wellbore. As it can be seen in the tip region compressive forces are vanished or are very small. On the sides of hydraulic fracture, compressive forces are higher and the lines showing compressive forces are radiating away from this region.

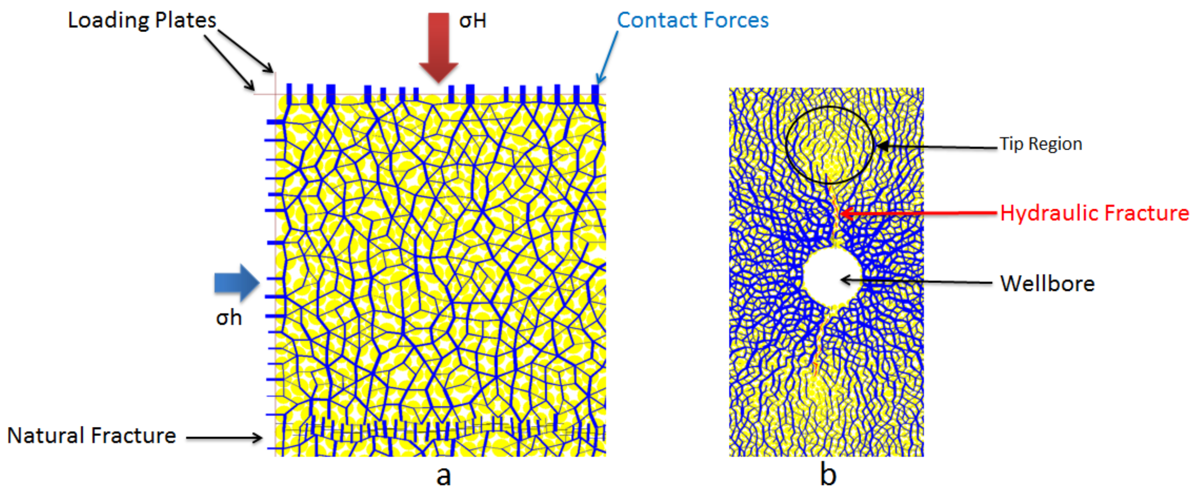

Figure 15: Compressive forces between particles. Blue lines represent contact forces. The thicker the lines,

the higher the contact force. (a) Upper left hand corner of sample. (b) Contact forces around wellbore after hydraulic fracture propagated some distance away from wellbore. At distances just beyond the tip of the fracture, compressive forces are either vanished or are very minor.

Figure 16 shows hydraulic fracture propagation, contact forces between particles and parallel bond forces for the case of 60° hydraulic and natural fracture interaction with cement as filling material. Compressive parallel bond forces are shown in blue colour and tensile parallel bond forces are shown in green colour. Figure 16a shows sample setup before borehole pressurization. Contact forces between particles and parallel bond forces are shown in Figure 16b and Figure 16c corresponding to sample state in Figure 16a. Figure 16b shows stress concentration around wellbore parallel to maximum horizontal stress and on the natural fractures. Figure 16d, Figure 16g and Figure 16j show hydraulic fracture propagation. In these three figures, natural fractures are not shown to be able to better observe shear slippage on natural fractures. Shear slippage is shown by red dashed lines on natural fractures. Figure 16(d, e and f) show hydraulic fracture half way between wellbore and natural fractures. Figure 16d shows that there is no shear slippage on natural fractures at this stage. Figure 16e shows that compressive forces are reduced to some extent around natural fractures. Figure 16f shows that parallel bond tensile forces didn’t reach natural fractures. Figure 16(g, h and i) show that hydraulic fracture didn’t intersect natural fractures but is very close to them. At this stage, shear slippage occurred on natural fractures. Figure 16h show that particle compressive forces are vanished on natural fractures ahead of hydraulic fracture tip. Figure 16i shows parallel bond tensile forces reached natural fractures. These tensile forces and particle movements caused shear slippage on the natural fracture. Figure 16(j, k and l) show the state of sample and forces after hydraulic fracture crossed natural fractures and hit the boundaries. Figure 16 showed the dynamic nature of hydraulic fracture propagation and its corresponding dynamic stress changes. Shear slippage on natural fractures occurred before hydraulic fracture intersects natural fractures. This doesn’t mean that shear slippage will always occur. It depends on the conditions of sample, natural fracture properties, stress state and fluid properties and flow rate. This shows that hydraulic fracturing is a dynamic process and should be simulated in this way. Trying to capture the physics of the problem and solving it in the static or pseudo-static manner can cause misleading results.

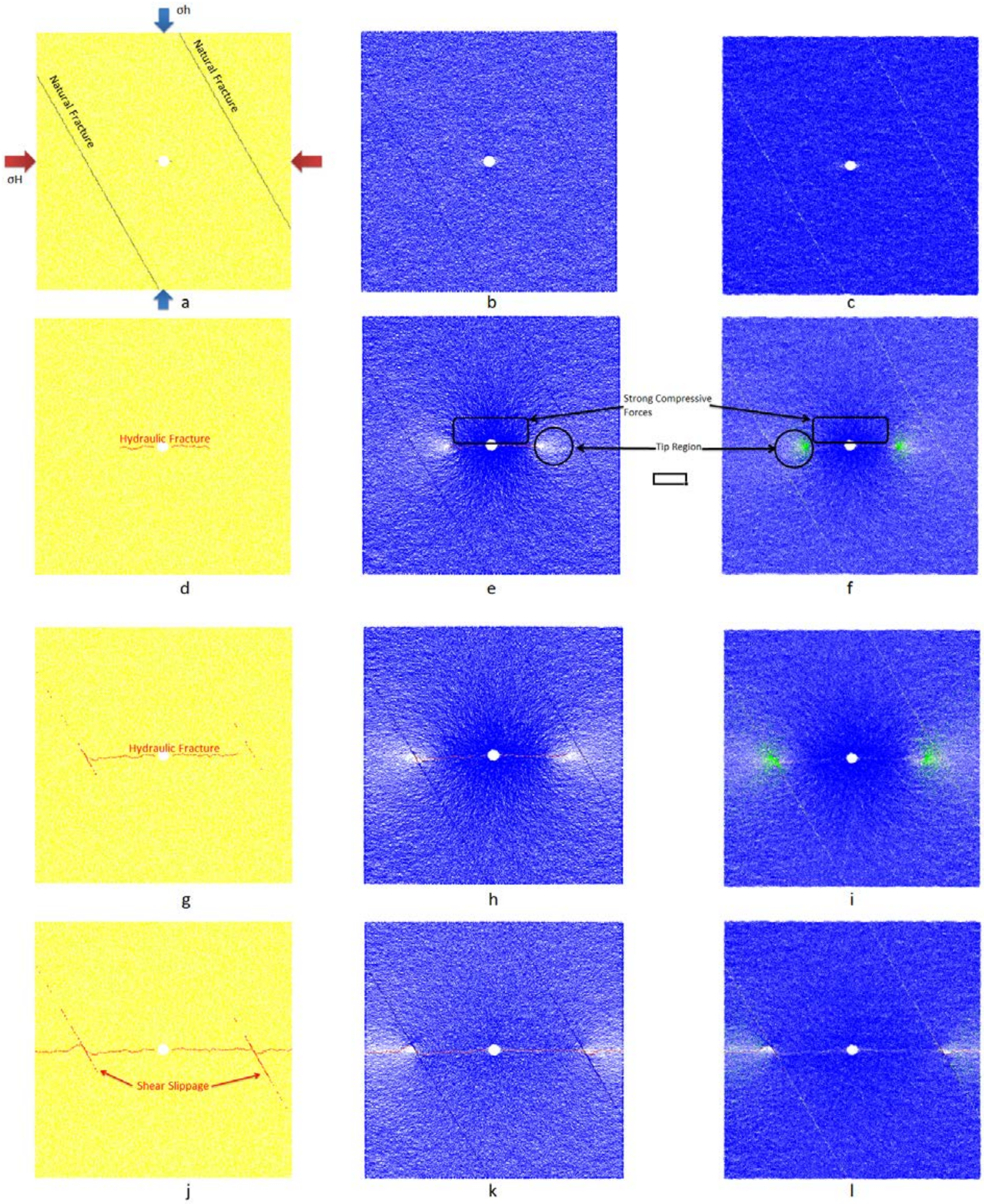

Figure 16: Hydraulic fracture propagation, contact and parallel bond forces and shear slippage on natural fractures for 60° fracture interaction angle with cement as filling material. (a) Sample set up before borehole pressurization. (b) Contact forces for sample in (a). (c) Parallel bond forces for sample in (a). (d) Hydraulic fracture propagated away from wellbore and half way to natural fractures. Natural fractures are

not shown in this figure. (e) Contact forces at the tip of hydraulic fracture are either vanished or are very small. These forces on the sides of hydraulic fracture are very strong. (f) Parallel bond forces at the tip of hydraulic fracture are tensile shown in green colour. Parallel bond forces on the sides of hydraulic fracture are very compressive. (g) Hydraulic fracture tip is very close to hit natural fractures but didn't intersect them yet. Hydraulic fracture caused shear slippage on the natural fracture surfaces. (h) Compressive forces ahead of Hydraulic fracture tip on the natural fracture are vanished. (i) Parallel bond force ahead of fracture tip and around natural fracture are tensile. (j, k, l) Hydraulic fracture crossed natural fractures.

Table 4 summarises the test parameters and results. This table also contains the test results predicted based on analytical criteria developed by Blanton (1986). Based on Blanton's theory, hydraulic fracture propagation stops momentarily once it interacts with natural fracture. Fracture pressurization inside wellbore, hydraulic fracture and intersection point will lead either to opening or crossing of natural fracture. If the condition of Equation 2 is satisfied, "crossing" will occur. Otherwise, "opening" will be the interaction result. In this equation "σ_H" and "σ_h" are maximum and minimum horizontal stresses respectiveley. "*T*" is the tensile strength of the rock. "*Θ*" is the interaction angle and "*b*" depend on the properties of natural fracture. More details about this analytical criteria can be found in Blanton's paper [7]. Using the properties of natural fracture and rock and the values of principal stresses in this study, test result were calculated and presented in Table 4.

$$\frac{\sigma_H - \sigma_h}{T} > \frac{-1}{Cos2\theta - bSin2\theta} \qquad \text{Equation 2}$$

Table 4 as well as the discussion above clearly indicate that simulation results can replicate the experimental condition; and be capable of producing the similar results. Results also indicate that simulation results match experimental results better than analytical results. The major difference between simulation and experiments is the 2D characteristic of the simulation. However, as discussed above, simulation is a better representation of field condition than experiments. The reason is that, in the simulation, there is no fluid leak off out of the sample from the plane perpendicular to vertical stress. This is similar to a reservoir formation that is sandwiched between two impermeable formations with higher stress contrast. Matrix permeability in the vertical direction doesn't allow excessive leak off to barrier formations contrary to what was observed in the experiments. In this case the fracture would be contained in the reservoir formation and the probability of fluid leak at formation interfaces would be very low. In the experiments, if the fracture arrives at top and bottom surfaces that are perpendicular to vertical stress, excessive fluid leak off could depressurize fluid causing excessive fluid energy loss which can significantly influence the outcome of the results. A remedy to this problem would be using samples with larger side lengths for experimental studies. But larger samples can introduce new problems. Creating synthetic homogenous large samples is very difficult. Handling and placement in the equipment and proper stress installation are involved with complex and tedious processes. If the opposing surfaces are not totally parallel, stress rotation and localization can jeopardize the results. Another difficulty with experimental studies is that these tests are extremely time consuming and require very expensive experimental setup. This puts constraint on the number of tests that can be done. As a result a strong conclusion that covers wide range of test conditions can be hardly possible to be drawn. Simulation studies can overcome these limitations to a large extent. Large scale simulated samples can easily be developed without affecting the homogeneity nature of the sample. Principal stresses can be controlled easily to make sure that there is no unwilling stress rotation. Tests can also be performed at a large frequency for a wide range of test conditions.

Table 4: Summary of test parameters and test results

			Interaction Results		
Test #	Natural fracture filling material	Interaction angle (^{o})	Simulation interaction result	Experimental Interaction Result	Analytical Criteria Blanton (1986)
1	Brown Glue	90	Arrest	Arrest	Cross
2	White Glue	30	Didn't intersect	Didn't intersect	Open
3	White Glue	60	Cross	Cross	Cross
4	Cement	0	Didn't intersect	Didn't intersect	Doesn't Interact
5	Cement	90	Cross	Cross-Arrest	Cross
6	Cement	60	Cross	Cross-Arrest	Cross
7	Cement	30	Arrest-Shear Slippage	Arrest-Shear Slippage	Open
	Principal stresses				

Test #	σ_v (psi)	σ_H (psi)	σ_h (psi)	Sample side length (cm)	Fluid Viscosity (cp)	Injection Rate (cc/min)
1	3000	2000	1000	10	97700	0.1
2	3000	2000	1000	10	97700	0.1
3	3000	2000	500	10	97700	0.1
4	3000	2000	1000	10	97700	0.1
5	3000	2000	1000	15	97700	0.1
6	3000	2000	1000	15	97700	0.1
7	3000	2000	1000	15	97700	0.1

It can be summarized based on previous discussion and Table 4 that the outcome of propagated hydraulic fracture and natural fracture interaction significantly depends on the orientation of natural fractures with respect to principal stresses and natural fractures filling material. Increasing the angle of natural fractures with respect to maximum horizontal stress increases the chance of crossing the natural fracture. Low angles between hydraulic fracture and natural fractures can cause shear slippage on the natural fracture planes. Filling material also plays a vital role. Weak planes increase the chance of shear slippage and arresting even at 90° orientation of natural fractures with respect to maximum horizontal stress as was observed in the case of brown glue filling material. If the filling material has strong cohesion strength such as the case of cement and white glue, they can resist shear slippage and aid the crossing behaviour at even lower angles of approach. In this study it was seen that at 60° angel of approach, hydraulic fracture crossed natural fractures when cement and white glue were used as filling materials. However, there are more parameters to be considered such as deviatoric stress (i.e. the difference of the magnitude of maximum and minimum horizontal stress), friction coefficient of natural fracture, fluid injection flow rate, fluid properties, as well as rock mechanical properties. In these tests, natural fractures were assumed to have large lengths and cross the sample boundaries. This was because of the difficulty to embed natural fractures in samples with desired surface properties to not cross the boundaries. In field cases, natural fracture lengths can be divided into three groups based on Daneshy's classification [16]. Based on his classification, natural flaws are small, medium or large. Small flaws have no effect on the propagation path. Medium flaws can cause small changes in propagation path but has no effect on the overall path. Large fractures can have significant effect on the propagation path depending on conditions such as being open or close, rock and fluid properties and stress condition. In the tests conducted in this study natural fractures belong to the third group.

7. Conclusion

This paper presented the results of experimental and numerical studies on the interaction of propagated hydraulic fracture with natural fractures. Three types of natural fracture filling materials have been tested. Experimental studies were performed on 10 and 15 cm prismatic synthetic mortar samples. Samples were tested in a True Triaxial Stress Cell, which has the capacity to facilitate application of three independent principal stresses on the test sample. The numerical simulation is carried out using Distinct Element Method (DEM) based numerical simulator tool, PFC2D. The purpose of the study was to validate simulation results by comparing them against experimental results. It was shown that simulation results were very similar to experimental results.

Both experimental and numerical results demonstrated that increasing the angle between the direction of maximum horizontal stress and natural fracture planes, increases the chance of propagated hydraulic fracture to cross natural fractures. The results also showed that natural fractures filling material plays a vital role on the interaction outcome. Weak filling materials increase the chance of shear slippage on natural fracture planes while increasing the strength of filling material increases the chance of crossing natural fractures.

Experimental results showed that if hydraulic fracture crosses the boundary that is orthogonal to vertical stress, it can cause a rapid depressurization of fracturing fluid resulting in rapid loss of fluid energy. This can affect the hydraulic and natural fractures interaction outcome, and cause arresting of hydraulic fracture at natural fracture planes. Numerical simulation was shown to handle this situation better and generate more accurate results.

Misaligned gluing of slabs to centre piece during preparation of testing sample can cause misleading interaction behaviour of natural and propagated hydraulic fracture, which warrant the importance of serious attention to careful preparation of testing sample. The chance of such error is relatively thin for numerical modelling. The simulation model was found to be better representation of the test scenario, which can generate more accurate results to interpret the interaction behaviour of natural and propagated hydraulic fractures.

Simulation model presented in this paper can be used to conduct more sensitivity analysis to study the effect of other parameters such as deviatoric stress, natural fracture size and orientation, and natural fracture permeability.

One of the limitations of the simulation model is the 2D characteristic of the model. However, this model still can help to better understand the interaction mechanism of propagated hydraulic and natural fracture. Further study can be pursued to extend the model to PFC3D to capture more accurately the 3D physics of the problem.

References

[1] C.T. Montgomery, M.B. Smith, Hydraulic Fracturing: History Of An Enduring Technology, (2010).

[2] N. Lamont, F.W. Jessen, The Effects of Existing Fractures in Rocks on the Extension of Hydraulic Fractures, (1963).

[3] G.D. Anderson, Effects of Friction on Hydraulic Fracture Growth Near Unbonded Interfaces in Rocks, (1981).

[4] M.E. Hanson, R.J. Shaffer, G.D. Anderson, Effects of Various Parameters on Hydraulic Fracturing Geometry, (1981).

[5] T.L. Blanton, An Experimental Study of Interaction Between Hydraulically Induced and Pre-Existing Fractures, in, Society of Petroleum Engineers, 1982.

[6] R.J. Shaffer, R.K. Thorpe, A.R. Ingraffea, F.E. Heuze, Numerical and Physical Studies of Fluid-Driven Fracture Propagation in Jointed Rock, in, Society of Petroleum Engineers, 1984.

[7] T.L. Blanton, Propagation of Hydraulically and Dynamically Induced Fractures in Naturally Fractured Reservoirs, in, Society of Petroleum Engineers, 1986.

[8] N.R. Warpinski, L.W. Teufel, Influence of Geologic Discontinuities on Hydraulic Fracture Propagation (includes associated papers 17011 and 17074), (1987).

[9] C.E. Renshaw, D.D. Pollard, An experimentally verified criterion for propagation across unbounded frictional interfaces in brittle, linear elastic materials, International Journal of Rock Mechanics and Mining Sciences & Geomechanics Abstracts, 32 (1995) 237-249.

[10] J. Zhou, M. Chen, Y. Jin, G.-q. Zhang, Analysis of fracture propagation behavior and fracture geometry using a tri-axial fracturing system in naturally fractured reservoirs, International Journal of Rock Mechanics and Mining Sciences, 45 (2008) 1143-1152.

[11] H. Gu, X. Weng, J.B. Lund, M.G. Mack, U. Ganguly, R. Suarez-Rivera, Hydraulic Fracture Crossing Natural Fracture at Non-Orthogonal Angles, A Criterion, Its Validation and Applications, in, Society of Petroleum Engineers, 2011.

[12] H. Gu, X. Weng, J.B. Lund, M.G. Mack, U. Ganguly, R. Suarez-Rivera, Hydraulic Fracture Crossing Natural Fracture at Nonorthogonal Angles: A Criterion and Its Validation, (2012).

[13] R.L. Johnson, Jr., B. Glassborow, M.P. Scott, Z.J. Pallikathekathil, A. Datey, J. Meyer, Utilizing Current Technologies to Understand Permeability, Stress Azimuths and Magnitudes and their Impact on Hydraulic Fracturing Success in a Coal Seam Gas Reservoir, in, Society of Petroleum Engineers, 2010.

[14] R.L. Johnson, M.P. Scott, R.G. Jeffrey, Z. Chen, L. Bennett, C.B. Vandenborn, S. Tcherkashnev, Evaluating Hydraulic Fracture Effectiveness in a Coal Seam Gas Reservoir from Surface Tiltmeter and Microseismic Monitoring, in, Society of Petroleum Engineers, 2010.

[15] M.P. Scott, R.L. Johnson, A. Datey, C.B. Vandenborn, R.A. Woodroof, Evaluating Hydraulic Fracture Geometry from Sonic Anisotropy and Radioactive Tracer Logs, in, Society of Petroleum Engineers, 2010.

[16] A.A. Daneshy, Hydraulic Fracture Propagation in the Presence of Planes of Weakness, in, Society of Petroleum Engineers, 1974.

[17] M. Thiercelin, E. Makkhyu, Stress Field In the Vicinity of a Natural Fault Activated By the Propagation of an Induced Hydraulic Fracture, in, American Rock Mechanics Association, 2007.

[18] H. Gu, X. Weng, Criterion For Fractures Crossing Frictional Interfaces At Non-orthogonal Angles, in, American Rock Mechanics Association, 2010.

[19] N.B. Nagel, M.A. Sanchez-Nagel, X. Garcia, B. Lee, A Numerical Evaluation of the Geomechanical Interactions Between a Hydraulic Fracture Stimulation And a Natural Fracture System, in, American Rock Mechanics Association, 2012.

[20] V. Sesetty, A. Ghassemi, Simulation of Hydraulic Fractures And Their Interactions With Natural Fractures, in, American Rock Mechanics Association, 2012.

[21] D. Chuprakov, O. Melchaeva, R. Prioul, Injection-Sensitive Mechanics of Hydraulic Fracture Interaction With Discontinuities, in, American Rock Mechanics Association, 2013.

[22] M. Cottrell, H. Hosseinpour, W. Dershowitz, Rapid Discrete Fracture Analysis of Hydraulic Fracture Development in Naturally Fractured Reservoirs, in, Society of Petroleum Engineers, 2013.

[23] F. Zhang, N. Nagel, F. Sheibani, Evaluation of Hydraulic Fractures Crossing Natural Fractures at High Angles Using a Hybrid Discrete-Continuum Model, in, American Rock Mechanics Association, 2014.

[24] K. Wu, J.E. Olson, Mechanics Analysis of Interaction Between Hydraulic and Natural Fractures in Shale Reservoirs, in, Society of Petroleum Engineers, 2014.

[25] A. Dahi Taleghani, J.E. Olson, How Natural Fractures Could Affect Hydraulic-Fracture Geometry, (2014).

[26] K. Wu, J.E. Olson, Numerical Investigation of Complex Hydraulic Fracture Development in Naturally Fractured Reservoirs, in, Society of Petroleum Engineers, 2015.

[27] R. Keshavarzi, R. Jahanbakhshi, Investigation of Hydraulic and Natural Fracture Interaction: Numerical Modeling or Artificial Intelligence?, in, International Society for Rock Mechanics, 2013.

[28] F.A. Tavarez, Discrete Element Method for Modeling Solid and Particulate Materials, University of Wisconsin--Madison, 2005.

[29] H. Fatahi, Simulation of Shale Mechanical Properties in PFC2d and Calibration of Them Against Lab Results for Tensile, Uni-Axial and Confined Compression Tests, in: SPE Annual Technical Conference and Exhibition, 27-29 October, Amsterdam, The Netherlands, Society of Petroleum Engineers, 2014, pp. 12.

[30] Itasca, Particle Flow Code in 2 Dimensions, Fourth ed., Itasca Consulting Group Inc. , 2008.

[31] H. Fatahi, M.M. Hossain, Fluid flow through porous media using distinct element based numerical method, Journal of Petroleum Exploration and Production Technology, (2015) 1-26.

[32] H. Fatahi, M.M. Hossain, S.H.F. Abarghooei, M. Mostofi, Numerical Simulation for the Determination of Hydraulic Fracture initiation and breakdown pressure using distinct element method, Submited for review, (2016).

[33] M. Sarmadivaleh, Experimental and numerical study of interaction of a pre-existing natural interface and an induced hydraulic fracture, Curtin University., 2012.

[34] M. Sarmadivaleh, V. Rasouli, Test design and sample preparation procedure for experimental investigation of hydraulic fracturing interaction modes, Rock Mechanics and Rock Engineering, 48 (2015) 93-105.

[35] E. Technology, Epoxy Adhesive Application Guide, in: E. Technology (Ed.), 2016.

[36] B. Haimson, C. Fairhurst, Hydraulic Fracturing in Porous-Permeable Materials, (1969).

[37] M.D. Zoback, F. Rummel, R. Jung, C.B. Raleigh, Laboratory hydraulic fracturing experiments in intact and pre-fractured rock, International Journal of Rock Mechanics and Mining Sciences & Geomechanics Abstracts, 14 (1977) 49-58.

[38] R.L. Aamodt, R.M. Potter, Anomalous Fracture-Extension Pressure In Granitic Rocks, in, American Rock Mechanics Association, 1978.

[39] C.M. Kim, K.E. Gray, Hydraulic Fracturing In Porous Rock With Particular Reference To Vertical Fracture Boundaries, in, American Rock Mechanics Association, 1978.

[40] W.L. Medlin, L. Masse, Laboratory Investigation of Fracture Initiation Pressure and Orientation, (1979).

[41] N.R. Warpinski, J.A. Clark, R.A. Schmidt, C.W. Huddle, Laboratory Investigation on the -Effect of In-Situ Stresses on Hydraulic Fracture Containment, (1982).

[42] L.W. Teufel, J.A. Clark, Hydraulic Fracture Propagation in Layered Rock: Experimental Studies of Fracture Containment, (1984).

[43] W.L. Medlin, L. Masse, Laboratory Experiments in Fracture Propagation, (1984).

[44] F.E. Heuze, R.J. Shaffer, A.R. Ingraffea, R.H. Nilson, Propagation of fluid-driven fractures in jointed rock. Part 1—development and validation of methods of analysis, International Journal of Rock Mechanics and Mining Sciences & Geomechanics Abstracts, 27 (1990) 243-254.

[45] S.C. Blair, R.K. Thorpe, F.E. Heuze, Propagation of fluid-driven fractures in jointed rock. Part 2—Physical tests on blocks with an interface or lens, International Journal of Rock Mechanics and Mining Sciences & Geomechanics Abstracts, 27 (1990) 255-268.

[46] M.D. Zoback, Reservoir Geomechanics, Cambridge University Press, 2010.

[47] C.J. de Pater, M.P. Cleary, T.S. Quinn, D.T. Barr, D.E. Johnson, L. Weijers, Experimental Verification of Dimensional Analysis for Hydraulic Fracturing, (1994).